PROCEEDINGS OF SCIENCE

Nuclear Spin Physics via Polarization Measurements

T. Wakasa*
Department of Physics, Kyushu University
E-mail: wakasa@phys.kyushu-u.ac.jp

One of the primary goals of nuclear physics is to describe nuclei and their dynamics in terms of interactions between nuclear constituents. In addition, high-precision experimental data and sophisticated calculations are very important for other research fields such as astrophysics and neutrino physics. Three topics are discussed by comparing experimental data with recent theoretical calculations; three-nucleon force effects in few nucleon systems, polarization phenomena and spin-isospin responses in quest of a comprehensive description of nuclei, and applications to neutrino physics.

23rd International Spin Physics Symposium - SPIN2018 -
10-14 September, 2018
Ferrara, Italy

*Speaker.

PoS(SPIN2018)005

1. Introduction

Recent progress in the nuclear spin physics via polarization measurements is reviewed with special emphases on three nucleon force effects, spin-isospin responses for unstable nuclei, and new spin-isospin modes and applications to neutrino physics. This progress has been made possible by the development of techniques such as heavy-ion charge exchange measurements, high quality polarized beams and targets, and sophisticated theoretical calculations.

2. Three nucleon force effects

2.1 Three nucleon force and chiral effective field theory

Three nucleon force (3NF) effect in nuclear many body systems is one of the hottest topics in nuclear physics. The first indication is the underbinding of theoretical calculations for ^{3}H and ^{3}He. Other indications are the binding and excitation energies for light nuclei. For example, in the Green-function Monte Carlo (GFMC) calculations [1], the calculation with the two nucleon forces (2NFs) is significantly underbinding compared with the experimental data. By introducing the 3NFs, the calculations become close to the data. It should be noted that different 3NF models such as Urbana [2] and Illinois [3] models give different predictions. Both forces include the so-called Fujita-Miyazawa 3NF [4] and the repulsive term. For the Illinois force, the three-pion (3π) ring diagrams are also considered [3], and give more attraction for neutron rich nuclei. Figure 1 shows a typical example for He isotopes. For ^{8}He, the Illinois model (AV18+IL7) with 3π-ring terms becomes more close to the experimental data. However, if we consider the general structure of 3NFs, we need 22 structure functions even under some invariance conditions [5]. Therefore, a systematic approach such as the chiral effective field theory (χEFT) is important.

Figure 2 shows the chiral expansion of nuclear forces [6]. The 2NF can be expanded as shown in the 2nd column; with some parameters to be determined experimentally by *NN* and π-*N* scattering data. Then, the 3NF appears at next-to-next leading order (N^{2}LO) as shown in the 3rd column. The left diagram corresponds to the 2π exchange Fujita-Miyazawa type, and its strength

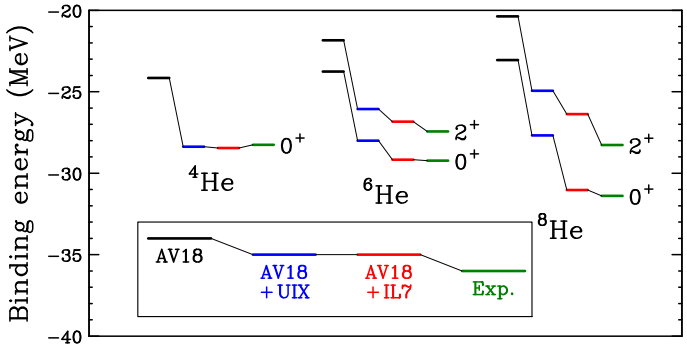

Figure 1: GFMC energies of ground 0^+ and excited 2^+ states for He isotopes with AV18 (black lines), AV18+UIX (blue lines), AV18+IL7 (red lines) Hamiltonians compared to experimental data (green lines) [1].

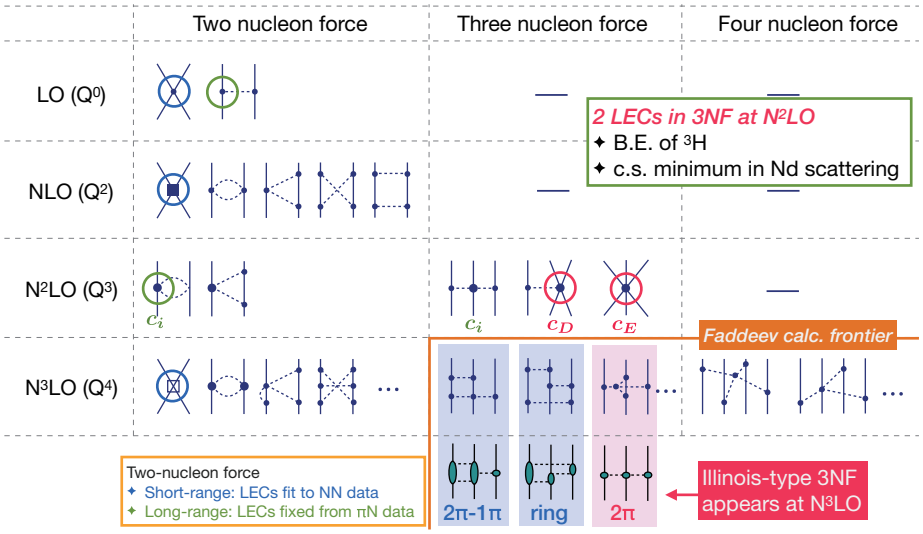

Figure 2: Schematic of chiral nuclear forces (2NF, 3NF, and four nucleon force) up to N^{3}LO [6]. Besides the πN low-energy constants (LECs) c_i, the 3NF diagrams at N^{2}LO contain two additional LECs: C_D and C_E. The 3π ring diagrams considered in the Illinois model [3] appear at N^{3}LO.

is determined by 2NF parameters. In this way, 2NF and 3NF can be derived consistently. There are another two diagrams for the 3NF at N^{2}LO, and corresponding parameters, C_D and C_E, should be determined independently by using the ^{3}H binding energy and p-d scattering data [7]. Recently, the Faddeev calculations using the chiral 2NF up to N^{4}LO become possible [8]. Furthermore, the calculations employing the chiral 2NF+3NF up to N^{2}LO are also available [7].

2.2 $T = 1/2$ three nucleon force

Many experimental data for p-d scattering have been accumulated. Figure 3(a) shows typical examples for the cross section data at 70 [9, 10], 135 [9–12], and 190 MeV [13]. The red curves represent the Faddeev calculations with the chiral 2NF up to N^{4}LO. Clear discrepancies are observed at cross section minima at $\theta_{\mathrm{c.m.}} \approx 120^\circ$. Epelbaum *et al.* [7] performed the calculations with the chiral 2NF+3NF up to N^{2}LO. Note that the 3NF parameters, C_D and C_E, have been determined at 70 MeV with the ^{3}H binding energy, and thus the results at higher energies are the parameter-free predictions. It is found that 3NF effects can remove the discrepancies between experimental data and theoretical calculations up to 135 MeV without adjustable parameter, and the discrepancies at higher energies would be due to higher-order ($>$ N^{2}LO) effects.

Figures 3(b) and 3(c)–(e) represent the vector and tensor analyzing powers for p-d elastic scattering, respectively, at 70 MeV (upper panels) [9, 10]. The red curves are the Faddeev calculations with the chiral 2NF up to N^{4}LO. Except for the tensor analyzing powers T_{21} and T_{22} at backward angles, a reasonable description within the theoretical uncertainty has been observed. Large discrepancies in T_{21} and T_{22} show the importance of the 3NF effects for these observables. Recent calculations with the chiral 2NF+3NF up to N^{2}LO [7] also suggest the importance of the higher-order ($>$ N^{2}LO) 3NF effects.

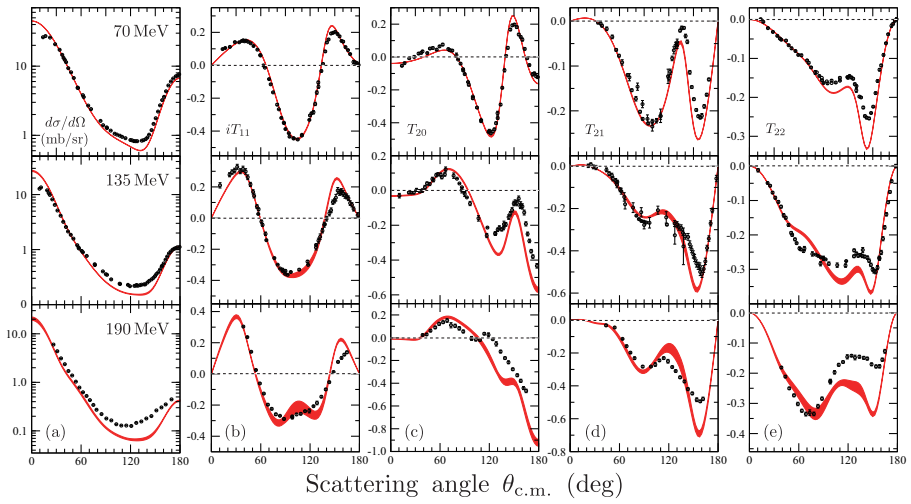

Figure 3: The cross sections [(a)] and the vector [(b)] and tensor [(c)–(e)] analyzing powers for *p-d* elastic scattering at 70 (upper panels) [9, 10], 135 (middle panels) [9–12], and 190 MeV (bottom panels) [13]. The red curves represent the Faddeev calculations with the chiral 2NF up to N^{4}LO [13].

Complete calculations for three-nucleon scattering states are limited up to N^{2}LO as of this moment. At the next N^{3}LO, there is no adjustable parameter. However, theoretically, large next fourth-order contributions are expected due to the Δ excitation [14]. Thus we should go to this order, and then there appear 10 new parameters [15]. In order to determine these parameters, high-precision *p-d* scattering data are needed in wide energy region for partial-wave analysis [6].

The middle and bottom panels of Fig. 3 show the cross sections [(a)] and the vector [(b)] and tensor [(c)–(e)] analyzing powers for *p-d* elastic scattering at 135 [9–12] and 190 MeV [13], respectively. The red curves represent the predictions with the chiral 2NF up to N^{4}LO. At these higher energies, the calculations generally different from the data at backward angles where 3NF effects become significant [16]. These high-precision data would be useful to determine the parameters for 3NFs at N^{4}LO. However, it should be noted that the total isospin T is limited to $1/2$ for the *p-d* scattering. Thus the four nucleon system such as *p*-^{3}He is attracting more attention for investigating the isospin $T = 3/2$ 3NF.

2.3 $T = 3/2$ three nucleon force

Recently, Viviani *et al.* [17] have succeeded the four-body calculations including the 3NF for *p*-^{3}He at 5.54 MeV. The analyzing power data and calculations suggest the importance of the 3π-ring 3NF included in the Illinois model [3]. Since this kind 3NF has a different isospin dependence compared with the Fujita-Miyazawa 3NF, the *p*-^{3}He data seem to be important to access the isospin dependence of the 3NFs. Thus it is important experimentally to measure these polarization observables at higher energies where the 3NF effects become more significant.

Watanabe *et al.* [18] have succeeded to measure the ^{3}He analyzing power $A_y(^3\mathrm{He})$ for *p*-^{3}He at 70 MeV. Figure 4 shows their preliminary results with the predictions employing the CD-Bonn [19]

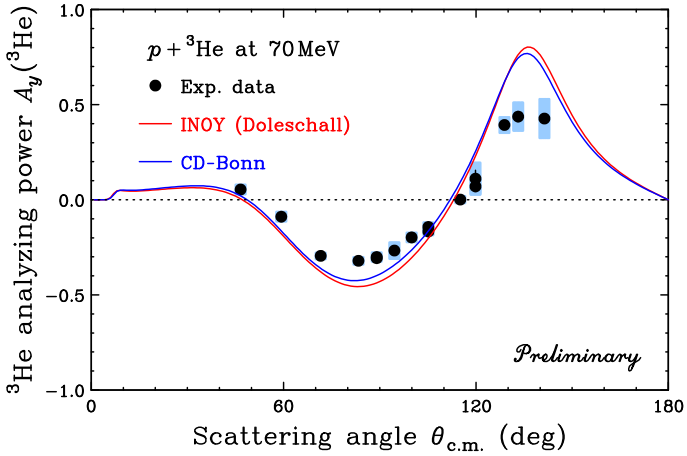

Figure 4: The ^{3}He analyzing power $A_y(^3\mathrm{He})$ for p-^{3}He at 70 MeV [18]. The error bars and boxes represent the statistical and systematic uncertainties, respectively. The blue and red lines are the theoretical calculations based on the CD-Bonn [19] and INOY (Doleschall) [20] 2NFs, respectively.

and INOY (Doleschall) [20] 2NFs. Significant discrepancies are observed at angles with minimum ($\theta_{\mathrm{c.m.}} \approx 80^\circ$) and maximum ($\theta_{\mathrm{c.m.}} \approx 140^\circ$) $A_y(^3\mathrm{He})$ values. At a low energy of 5.54 MeV, the 3NF effect is only about 0.05 [17]. The present data suggest the increase of the 3NF effect to about 0.2. Even though we must await a calculation including the 3NF in near future, these experimental data would be helpful to investigate the isospin $T = 3/2$ 3NF.

3. Spin-isospin responses

3.1 Gamow-Teller resonance

A giant resonance (GR) is a collective oscillation mode of an atomic nucleus and also a feature of quantum many-body systems [21]. At low momentum transfers, the Gamow-Teller (GT) giant resonance (GTGR) is excited and the relevant repulsive interaction is often described by the Landau-Migdal parameter g' [1] [22, 23]. The Landau-Migdal parameter g' is a key parameter to understand the GT response, and it is almost constant for stable nuclei [24]. Recently, the GT responses for unstable nuclei have been extensively studied by using the inverse (p,n) reaction at NSCL [25, 26] and RIBF [27, 28]. The GT resonances (GTRs) have been successfully observed for very neutron rich nuclei such as ^{8}He [27] and ^{12}Be [28]. Furthermore, the GTGR has been successfully observed for ^{132}Sn [29]. These nuclei are far from stability, and thus valuable for understanding the isospin dependence of the GT responses.

3.1.1 ^{132}Sn

The ^{132}Sn is the double-magic nucleus between well-studied ^{90}Zr and ^{208}Pb nuclei. Therefore, the data are very useful to benchmark the nuclear models in medium-heavy region. Furthermore,

[1] $g' = g'_{NN}$ in Ref. [24].

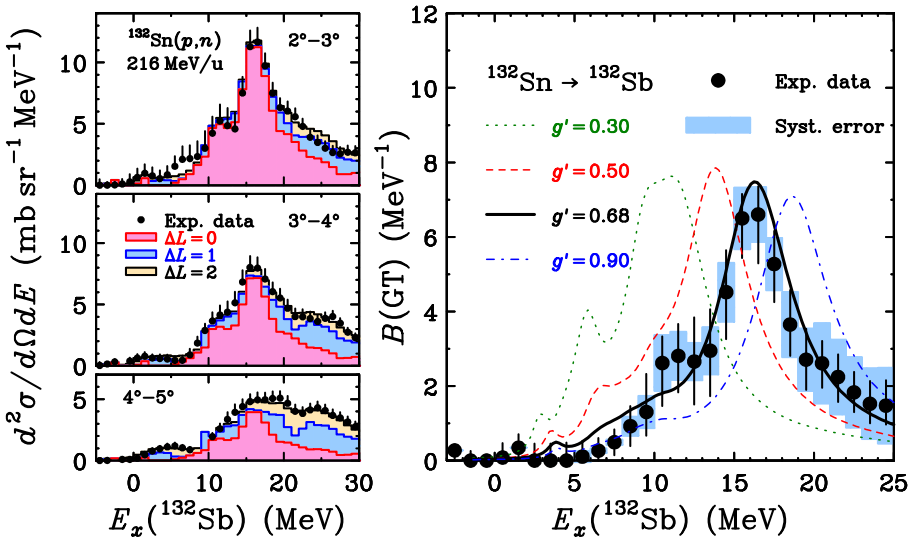

Figure 5: (Left) the cross sections and the results of the MDA for the ^{132}Sn(p,n) reaction at 216 MeV/u [29]. (Right) GT strength distribution in ^{132}Sn compared with the RPA calculations employing different g' values of 0.30, 0.50, 0.68, and 0.90.

Sn has a very-long isotope chain, and thus is suitable to investigate the isospin dependence of the GT peak which is sensitive to the Landau-Migdal parameter g'.

The experiment was performed at RIBF in RIKEN. The secondary ^{132}Sn beam bombarded an 11 mm thick liquid hydrogen target, and the neutrons from the (p,n) reaction were measured by the WINDS neutron detectors [30]. The resulting Sb isotopes were momentum-analyzed by the SAMURAI spectrometer [31] with wide momentum acceptance of about 50%.

The experimental results for the cross sections at $\theta_{\rm c.m.} = 2°$–$5°$ are shown in Fig. 5. The data have been decomposed to Gamow-Teller ($\Delta L = 0$), dipole ($\Delta L = 1$), and quadrupole ($\Delta L = 2$) components by multi-pole decomposition (MDA). At most forward angle, the prominent GTGR is clearly seen at about 16 MeV. Furthermore, the spin-dipole resonance is also found at about 25 MeV. The GT cross section $\sigma_{\Delta L=0}(q,\omega)$ has been converted to the GT strength B(GT) by using the following proportionality relation:

$$\sigma_{\Delta L=0}(q,\omega) = \hat{\sigma}_{\rm GT} F(q,\omega) B({\rm GT}), \tag{3.1}$$

with the GT unit cross section $\hat{\sigma}_{\rm GT}$ and the (q,ω) dependence factor $F(q,\omega)$.

The right panel of Fig. 5 compares the experimental GT strength distribution with theoretical predictions for different Landau-Migdal parameters g'. The experimental data are best reproduced with the g' value of 0.68 shown by black. This value is close to the values evaluated from the ^{90}Zr [32] and ^{208}Pb [33] data. Therefore, the result shows the constancy of g' in the wide nuclear chart region up to isospin asymmetry $(N-Z)/A$ of 0.24. Note that the observed total strength corresponds to about 56% of the sum-rule value of $3(N-Z) = 96$. This value is consistent with the systematics for stable nuclei [24]. Since the excitation energy is limited up to 25 MeV, a future study for higher excitations is interesting to search for the missing strength.

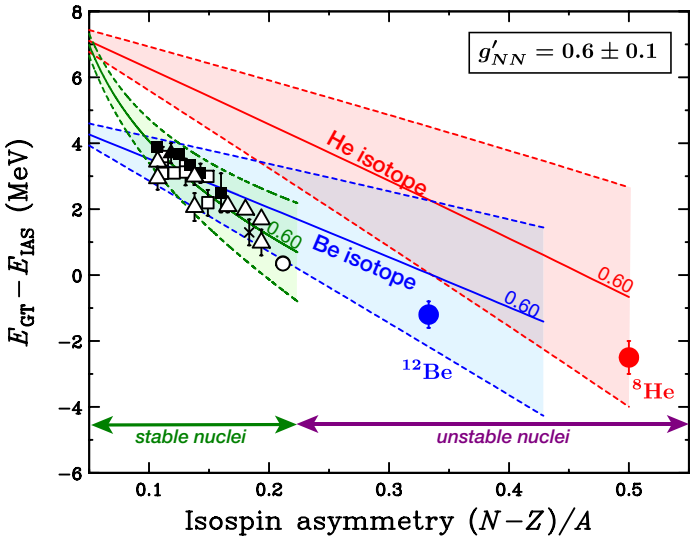

Figure 6: The energy difference between GTR and IAS, $E_{\rm GT} - E_{\rm IAS}$, as a function of isospin asymmetry $(N-Z)/A$. The data for stable nuclei with $(N-Z)/A \leq 0.21$ are taken from Ref. [34]. The red and blue circles represent the results for ^{8}He [27] and ^{12}Be [28], respectively. The bands are the theoretical predictions assuming the constant g' of 0.6 ± 0.1.

3.1.2 ^{8}He and ^{12}Be

A neutron-rich nucleus ^{8}He has the largest isospin asymmetry $(N-Z)/A$ of 0.5, and ^{12}Be has also a large asymmetry of 0.33. Therefore, for these very neutron-rich nuclei, it is very interesting to investigate how to change the repulsive spin-isospin interaction, g', by observing the GTRs.

The energy difference between GTR and isobaric-analog state (IAS) is given by [34]

$$E_{\rm GT} - E_{\rm IAS} = \Delta E_{ls} + {\rm const.}(g' - f')\frac{(N-Z)}{A}, \tag{3.2}$$

with Landau-Migdal parameters g' and f'. Thus the energy differences would be proportional to isospin asymmetry. Figure 6 shows the results for stable nuclei from Zr to Pb. The data support the constancy of g' of about 0.6, and the curvature is due to the shell effect in ΔE_{ls} [35]. Therefore, experimental data for ^{8}He and ^{12}Be are interesting to check whether the constancy of g' is hold or not up to a large isospin-asymmetry of 0.5.

First (p,n) measurements for these nuclei in inverse kinematics have been successfully performed at RIBF in RIKEN. In both cases, GTRs are clearly observed, and the energy differences from the IAS were determined as -2.5 MeV for ^{8}He [27] and -1.2 MeV for ^{12}Be [28].

In Fig. 6, new data for ^{8}He and ^{12}Be are shown by red and blue circles, respectively. The light red and blue bands correspond to the theoretical predictions assuming the constant Landau-Migdal parameter g' of 0.6 ± 0.1 for He and Be isotopes. The difference is due to the different spin-orbit splitting between He and Be. Both data are consistent with the predictions; therefore, the Landau-Migdal parameter g' would be constant up to isospin asymmetry $(N-Z)/A$ of 0.5. In these neutron-rich light nuclei, halo and cluster effects might affect the resonance energies. Thus we need further theoretical investigations to confirm the constancy of the residual interaction.

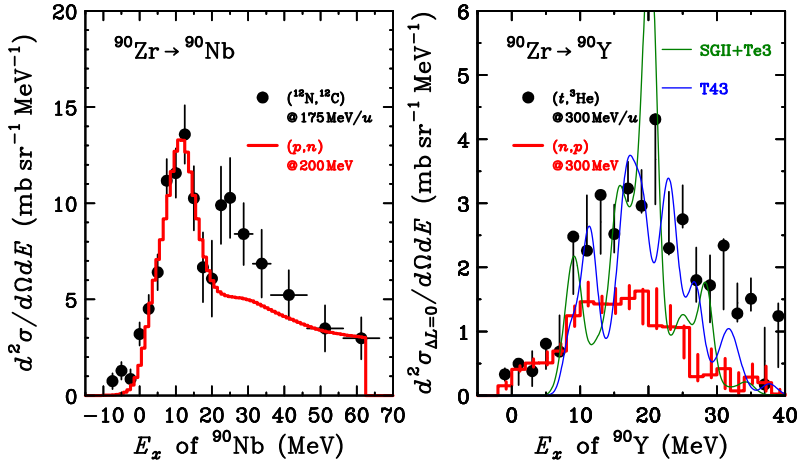

Figure 7: The cross section (left) and the monopole ($\Delta L = 0$) cross section (right) for the ^{90}Zr(^{12}N, ^{12}C) [37] and ^{90}Zr$(t,{}^3$He) [36] reactions at 0°. The red histograms are the relevant (p,n) [39] and (n,p) [40] data at 200 and 300 MeV. Hartree-Fock plus random-phase approximation (HF-RPA) calculations using the Skyrme effective interaction SGII+Te3 [41] and T43 [42] are shown by the green and blue lines, respectively.

3.2 Isovector spin-monopole resonance

The isovector spin-monopole (IVSM) is a breathing mode including spin-isospin degrees of freedom and its operator, $O^{\rm IVSM}_{\pm}(\mu)$ $\sum_k t_{\pm}(k)\sigma_{\mu}(k)r(k)^2$, has a r^2 term. There is the model-independent sum-rule for the total strengths $S_{\pm}$ [21]. The difference of the total strength in the β^- and β^+ directions is given by

$$S_- - S_+ = 3(N\langle r^4\rangle_n - Z\langle r^4\rangle_p), \tag{3.3}$$

with the neutron and proton distributions in nuclei. This sum-rule value is sensitive to the neutron skin because of the fourth-power for r. Therefore, the IVSM would be useful to obtain the neutron skin thickness and to constrain the nuclear matter equation-of-state.

Experimentally, an appropriate probe sensitive to the IVSM mode should be selected. One promising tool is the heavy-ion charge exchange reactions such as using triton [36] and nitrogen [37] beams. In the radial dependence of the transition density, there is a node near the surface, and thus the cancellation between the inner and surface regions occurs for the nucleon charge exchange reaction [38]. However, due to the strong absorption, heavy-ion-induced reactions probe only the surface region, and thus there is no cancellation. Therefore, the IVSM mode would be effectively excited.

The left panel of Fig. 7 shows the experimental result for the β^- direction on ^{90}Zr [37] as a function of excitation energy. For comparison, the (p,n) spectrum at 200 MeV [39] is also shown by the red histogram. The GTGR at about 10 MeV is clearly observed for both cases. In contrast to the (p,n) case, there is an another resonance at about 25 MeV. This resonance would be the IVSM resonance and the data clearly demonstrate the suitability of this probe for the monopole resonance. The right panel shows the result for the β^+ direction [36]. In this case, the significant enhancement

from the (n,p) data [40] is also observed at about 20 MeV, and this enhancement is consistent with the theoretical predictions using the Skyrme effective interactions [41, 42].

From these cross sections, the monopole strengths are deduced by using the empirical proportionality relation similar to Eq. (3.1) between the strength and the cross section. The finally obtained integrated monopole strengths are

$$S_- = (25 \pm 6) \times 10^3\,\mathrm{fm}^4, \quad S_+ = (16 \pm 6) \times 10^3\,\mathrm{fm}^4. \tag{3.4}$$

Thus the spin-monopole sum-rule value becomes about $9 \times 10^3\,\mathrm{fm}^4$, and the neutron skin thickness can be deduced as $\delta_{np} = 0.10 \pm 0.16\,\mathrm{fm}$. The uncertainty is relatively large; however, the present value is consistent with other works [43, 44]. The present accuracy is limited by both the experimental statistics and the theoretical uncertainty. Thus the future experiment with more intense beams and theoretical investigations would enable us to obtain more accurate information about the IVSM mode.

4. New spin-isospin modes and applications to neutrino physics

4.1 $0\nu\beta\beta$ decay and double charge-exchange reaction

The spin-isospin responses are also important in relation to zero-neutrino (0ν) double-beta ($\beta\beta$) decay. The relation between the $0\nu\beta\beta$ decay half-life $T_{1/2}^{0\nu\beta\beta}$ and the neutrino effective mass $\langle m_\nu \rangle$ is given by

$$\left[T_{1/2}^{0\nu\beta\beta}(0^+ \to 0^+)\right]^{-1} = G_{0\nu} M^{0\nu\beta\beta} \left(\frac{\langle m_\nu \rangle}{m_e}\right)^2, \tag{4.1}$$

and thus we need the nuclear matrix element $M^{0\nu\beta\beta}$ to deduce $\langle m_\nu \rangle$. Because we could not obtain this nuclear matrix element experimentally, we need nuclear structure calculations to obtain $M^{0\nu\beta\beta}$. There are several nuclear-model calculations from ^{48}Ca to ^{150}Nd, and the model dependence is significantly large by a factor of two [45]. One candidate for the experimental constraint to $M^{0\nu\beta\beta}$ is the double GT (DGT) excitation by double charge-exchange (DCX) reaction, since the relevant operators are very similar as follows except for the neutrino potential V_{GT}:

$$\hat{O}_{\mathrm{GT}}^{0\nu} = \sum_{i<j} V_{\mathrm{GT}} \sigma_i \sigma_j \tau_i^- \tau_j^-, \quad \hat{O}_{\mathrm{GT}}^{\mathrm{DCX}} = \sum_{i<j} [\sigma_i \tau_i^- \times \sigma_j \tau_j^-]^0. \tag{4.2}$$

Theoretically, almost linear correlation between 0ν and DGT matrix elements is predicted [45]; therefore, DCX reactions would provide the information on $M^{0\nu\beta\beta}$ experimentally.

The DCX ^{40}Ca(^{18}O, ^{18}Ne)^{40}Ar reaction was measured at 270 MeV at INFN-LNS [46], and the $^{40}\mathrm{Ca}(0^+) \to {}^{40}\mathrm{Ar}(0^+)$ transition has been clearly observed. This transition includes both DGT and double Fermi (DF) transitions, since both transitions can excite the 0^+ state with $\Delta L = 0$. Each contribution can be factorized as

$$\sigma(0^\circ) = \sigma_{\mathrm{DGT}} + \sigma_{\mathrm{DF}} = \hat{\sigma}_{\mathrm{DGT}} F_{\mathrm{DGT}} B_P(\mathrm{DGT}) B_T(\mathrm{DGT}) + \hat{\sigma}_{\mathrm{DF}} F_{\mathrm{DF}} B_P(\mathrm{DF}) B_T(\mathrm{DF}), \tag{4.3}$$

where $\hat{\sigma}$ is the so-called unit cross section and B_P and B_T are projectile and target transition strengths, respectively. Under the following assumption between DGT and DF transitions:

$$B(\mathrm{DGT}) : B(\mathrm{DF}) = \sum_m B(\mathrm{GT}^-) B(\mathrm{GT}^+) : \sum_m B(\mathrm{F}^-) B(\mathrm{F}^+), \tag{4.4}$$

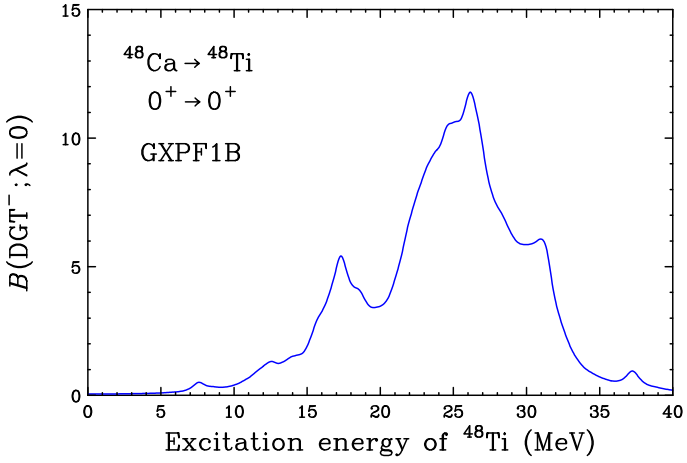

Figure 8: DGT strength distribution of ^{48}Ca to ^{48}Ti for $\lambda = 0$ ($0^+ \to 0^+$) [52] with the pf-shell GXPF1B nuclear interaction [53].

the nuclear matrix element for ^{40}Ca can be evaluated as $M^{0\nu\beta\beta}(^{40}\mathrm{Ca}) = 0.37 \pm 0.18$. Then, by correcting the Pauli blocking effects, the matrix element for ^{48}Ca can be estimated as $M^{0\nu\beta\beta}(^{48}\mathrm{Ca}) = 2.6 \pm 1.3$ [46]. This result is consistent with the theoretical prediction of 2.28 [47], and thus the reaction analysis seems to be reliable. Although we need further investigations to reduce the uncertainty, this method would be useful to constrain the $0\nu\beta\beta$ decay nuclear matrix elements experimentally.

4.2 Double GT resonance

The two-neutrino (2ν) $\beta\beta$ ($2\nu\beta\beta$) decay nuclear matrix elements $M^{2\nu\beta\beta}$ deduced from the half-life $T^{2\nu\beta\beta}_{1/2}$ exhaust only about 0.1% of the sum-rule value [48] and the situation is similar to delay of the single beta-decay. Thus we can expect naively that the missing strength would be found as the DGT resonance predicted thirty years ago [49]. For the double IAS, the (π^+, π^-) reaction successfully observed at $E_x = 17.38\,\mathrm{MeV}$ [50]. However, this probe is almost insensitive for the excitation of the double spin-flip GT state.

Recently, new idea to use the heavy-ion DCX reaction has been realized at RCNP by using the ^{12}C beam [51]. The outgoing ^{12}Be particles from the DCX reaction on ^{48}Ca were momentum-analyzed by the Grand-Raiden spectrometer. The final 0^+ state of ^{12}Be was identified by gamma-ray tagging. The projectile transition strength is large and thus the DGT state could be efficiently excited. Two prominent peaks have been observed at $E_x \approx 17$ and 27 MeV. The lower peak is relatively narrow, and thus would be the one-phonon single GT resonance. The other peak is more significant and broad, and thus a candidate of the two-phonon DGT resonance.

Figure 8 shows the shell-model prediction [52] for the DGT strength with the pf-shell GXPF1B nuclear interaction [53]. The calculation reasonably reproduces the experimentally observed double peak structure. Furthermore, the peak positions are consistent with the experimental data. Theoretically, the DGT distribution is sensitive to the paring correlation, and the $M^{0\nu\beta\beta}$ is also sensitive to this correlation [52]. The present data suggest the small paring correlation. The experimental

data are still preliminary; however, this heavy-ion DCX reaction would be useful to constrain the theoretical calculations for $M^{0\nu\beta\beta}$, and also to observe the DGT resonance.

5. Summary and outlook

Recent progress in the nuclear spin physics was reviewed. For 3NF effects in few nucleon systems, high quality data are accumulating for various systems and spin observables. At the moment the calculations based on the χEFT are at N^{2}LO for the 3NFs, and there are some discrepancies between experimental data and calculations. Thus the chiral expansion to the fourth-order is required, and we need both more systematic data for *p-d* elastic scattering for partial-wave analysis and the data for four nucleon systems for investigating the isospin $T = 3/2$ 3NFs. For the spin-isospin responses, the GTRs are observed both for very neutron rich nuclei such as ^{8}He and the double-magic nucleus of ^{132}Sn. These results suggest the constancy of the spin-isospin residual interaction in wide nuclear chart region for mass number A and isospin-asymmetry $(N-Z)/A$. However, we need further investigations especially for the total strength and higher multipole modes such as the spin-dipole response. For heavy-ion induced reactions, the IVSM resonances are clearly observed and the sum-rule value would provide another way to obtain the neutron skin thickness. Furthermore, double charge-exchange reactions could give a valuable constraint on the $0\nu\beta\beta$ decay nuclear matrix elements, and also very useful to observe new collective motions such as the DGT resonance.

Acknowledgments

I am grateful to K. Sekiguchi, K. Yako, M. Sasano, S. Noji, K. Miki, and M. Takaki for their valuable comments and help in preparing the presentation. I also acknowledge all collaborators of the relevant experiments performed at RCNP and RIKEN.

References

[1] J. Carlson *et al.*, *Rev. Mod. Phys.* **87** (2015) 1067.

[2] B.S. Pudliner *et al.*, *Phys. Rev. Lett.* **74** (1995) 4396.

[3] S.C. Pieper *et al.*, *Phys. Rev. C* **64** (2001) 014001.

[4] J. Fujita and H. Miyazawa, *Prog. Theor. Phys.* **17** (1957) 360.

[5] H. Krebs, A. Gasparyan, and E. Epelbaum, *Phys. Rev. C* **87** (2013) 054007.

[6] E. Epelbaum, *Chiral EFT for nuclear forces: State of the art and future perspectives*, in *YKIS2018b Symposium on Recent Developments in Quark-Hadron Sciences*, Kyoto, Japan (2018).

[7] E. Epelbaum *et al.*, *arXiv*:1807.02848[nucl-th].

[8] S. Binder *et al.*, *Phys. Rev. C* **93** (2016) 044002.

[9] K. Sekiguchi *et al.*, *Phys. Rev. C* **65** (2002) 034003.

[10] K. Suda *et al.*, *Nucl. Instrum. Methods Phys. Res. A* **572** (2007) 745.

[11] N. Sakamoto *et al.*, *Phys. Lett. B* **367** (1996) 60.

[12] H. Sakai *et al.*, *Phys. Rev. Lett.* **84** (2000) 5288.

[13] K. Sekiguchi *et al.*, *Phys. Rev. C* **96** (2017) 064001.

[14] E. Epelbaum, *Chiral three-nucleon force*, IHEP, Peking, September 2 (2014).

[15] L. Girlanda, A. Kievsky, and M. Viviani, *Phys. Rev. C* **84** (2011) 014001.

[16] H. Witała *et al.*, *Phys. Rev. Lett.* **81** (1998) 1183.

[17] M. Viviani *et al.*, *Phys. Rev. Lett.* **111** (2013) 172302.

[18] A. Watanabe *et al.*, *CYRIC Annual Report* 2016–2017, CYRIC, Tohoku University, in press.

[19] R. Machleidt, *Phys. Rev. C* **63** (2001) 024001.

[20] P. Doleschall, *Phys. Rev. C* **69** (2004) 054001.

[21] M.N. Harakeh and A. van der Woude, *Giant Resonances: Fundamental High-Frequency Modes of Nuclear Excitations*, Oxford University Press, New York, (2002).

[22] A.B. Migdal, *Rev. Mod. Phys.* **50** (1978) 107.

[23] J. Meyer-Ter-Vehn, *Phys. Rep.* **74** (1981) 323.

[24] M. Ichimura, H. Sakai, and T. Wakasa, *Prog. Part. Nucl. Phys.* **56** (2006) 446.

[25] M. Sasano *et al.*, *Phys. Rev. Lett.* **107** (2011) 202501.

[26] M. Sasano *et al.*, *Phys. Rev. C* **86** (2012) 034324.

[27] M. Kobayashi *et al.*, *JPS Conf. Proc.* **1** (2014) 013034.

[28] K. Yako *et al.*, *RIKEN Accel. Prog. Rep.* **45** (2012) v.

[29] J. Yasuda *et al.*, *Phys. Rev. Lett.* **121** (2018) 132501.

[30] K. Yako *et al.*, *RIKEN Accel. Prog. Rep.* **45** (2012) 137.

[31] T. Kobayashi *et al.*, *Nucl. Instrum. Methods Phys. Res. Sect. B* **317** (2013) 294.

[32] T. Wakasa, M. Ichimura, and H. Sakai, *Phys. Rev. C* **72** (2005) 067303.

[33] T. Wakasa *et al.*, *Phys. Rev. C* **85** (2012) 064606.

[34] K. Nakayama *et al.*, *Phys. Lett. B* **114** (1982) 217.

[35] A. Bohr and B.R. Mottelson, *Nuclear Structure Volume I: Single-Particle Motion*, Benjamin, New York, 1969.

[36] K. Miki *et al.*, *Phys. Rev. Lett.* **108** (2012) 262503.

[37] S. Noji *et al.*, *Phys. Rev. Lett.* **120** (2018) 172501.

[38] D.L. Prout *et al.*, *Phys. Rev. C* **63** (2000) 014603.

[39] C. Gaarde, *Nucl. Phys. A* **396** (1983) 127.

[40] K. Yako *et al.*, *Phys. Lett. B* **615** (2005) 193.

[41] C.L. Bai *et al.*, *Phys. Rev. C* **83** (2011) 054316.

[42] T. Lesinski *et al.*, *Phys. Rev. C* **76** (2007) 014312.

[43] L. Ray *et al.*, *Phys. Rev. C* **18** (1978) 1756.

[44] A. Trzcińska *et al.*, *Phys. Rev. Lett.* **87** (2001) 082501.

[45] J. Engel and J. Menéndez, *Rep. Prog. Phys.* **80** (2017) 046301.

[46] F. Cappuzzello *et al.*, *Eur. Phys. J. A* **51** (2015) 145.

[47] J. Area *et al.*, *Phys. Rev. Lett.* **109** (2012) 042501.

[48] E. Caurier *et al.*, *Phys. Lett. B* **711** (2012) 62.

[49] P. Vogel *et al.*, *Phys. Lett. B* **212** (1988) 259.

[50] M. Kaletka *et al.*, *Phys. Lett. B* **199** (1987) 336.

[51] M. Takaki *et al.*, *JPS Conf. Proc.* **6** (2015) 020038.

[52] N. Shimizu, J. Menéndez, and K. Yako, *Phys. Rev. Lett.* **120** (2018) 142502.

[53] M. Honma *et al.*, *RIKEN Accel. Prog. Rep.* **41** (2008) 32.